Hyperfine Interact (2016) 237: 43
DOI 10.1007/s10751-016-1281-x

Synchrotron radiation based Mössbauer absorption spectroscopy of various nuclides

Ryo Masuda[1] · Yasuhiro Kobayashi[1] · Shinji Kitao[1] · Masayuki Kurokuzu[1] · Makina Saito[1] · Yoshitaka Yoda[2] · Takaya Mitsui[3] · Makoto Seto[1,3]

Published online: 22 February 2016

Abstract Synchrotron-radiation (SR) based Mössbauer absorption spectroscopy of various nuclides is reviewed. The details of the measuring system and analysis method are described. Especially, the following two advantages of the current system are described: the detection of internal conversion electrons and the close distance between the energy standard scatterer and the detector. Both of these advantages yield the enhancement of the counting rate and reduction of the measuring time. Furthermore, SR-based Mössbauer absorption spectroscopy of ^{40}K, ^{151}Eu, and ^{174}Yb is introduced to show the wide applicability of this method. In addition to these three nuclides, SR-based Mössbauer absorption spectroscopy of ^{61}Ni, ^{73}Ge, ^{119}Sn, ^{125}Te, ^{127}I, ^{149}Sm, and ^{189}Os has been performed. We continue to develop the method to increase available nuclides and to increase its ease of use. The complementary relation between the time-domain method using SR, such as nuclear forward scattering and the energy-domain methods such as SR-based Mössbauer absorption spectroscopy is also noted.

Keywords Synchrotron radiation · Synchrotron-radiation based Mössbauer absorption spectroscopy · ^{40}K · ^{151}Eu · ^{174}Yb · Nuclear resonant inelastic scattering

This article is part of the Topical Collection on *Proceedings of the International Conference on the Applications of the Mössbauer Effect (ICAME 2015), Hamburg, Germany, 13-18 September 2015*

✉ Ryo Masuda
masudar@rri.kyoto-u.ac.jp

[1] Research Reactor Institute, Kyoto University, Kumatori-cho, Sennan-gun, Osaka 590-0494, Japan

[2] Resarch and Utilization Division, Japan Synchrotron Radiation Research Institute, Sayo-cho, Sayo-gun, Hyogo 679-5198, Japan

[3] Condensed Matter Science Division, Sector of Nuclear Science Research, Japan Atomic Energy Agency, Sayo-cho, Sayo-gun, Hyogo 679-5148, Japan

1 Introduction

Mössbauer spectroscopy is a powerful and established method in various fields, from fundamental studies to industrial applications [1]. Most Mössbauer studies have been performed using ^{57}Fe and ^{119}Sn, although the Mössbauer effect has been observed for 86 nuclides of 45 elements [2]. One large difficulty in Mössbauer spectroscopy is in the preparation of appropriate γ-ray sources. While sources for ^{57}Fe and ^{119}Sn are commercially available, the γ-ray source for the other nuclides needs to be synthesized on your own by an appropriate nuclear reaction. Moreover, in some cases like ^{40}K, there are no appropriate radioactive isotopes (RI) for its γ-ray source.

Synchrotron radiation (SR) is an alternative source for Mössbauer spectroscopy and it enables Mössbauer experiments of various nuclides. It may also realize the experiments with nuclides that do not have appropriate γ-ray sources. Actually, many Mössbauer experiments of various nuclides have been performed by the nuclear forward scattering (NFS) method [3], to observe their hyperfine structure. For example, NFS experiments of ^{40}K [4], and ^{187}Os [5], which were inaccessible by usual γ-ray sources, were successfully conducted. In NFS experiments, the time spectrum of NFS is observed and the hyperfine structure of the specific nuclide is obtained from the beat pattern of the time spectrum (quantum beat). Because the period of the quantum beat is typically greater than nanoseconds, the Si avalanche photodiode (APD) detector is usually used owing to its fast time response and high dynamic range. However, the detection efficiency of APD detectors for high energy X-rays is low. For example, the efficiency of the APD detector with a 150 μm depletion layer at 50 keV is below 1.5 %. Still, the NFS was successfully performed with nuclides whose resonant energy is high, such as ^{61}Ni [6] (Nuclear resonance energy $E_{\rm res}$ =67.4 keV) and ^{99}Ru ($E_{\rm res}$ =89.4 keV) [7], by using the multi-element APD detector and optimizing its arrangement.

Recently, SR-based Mössbauer absorption spectroscopy has been developed as another method for Mössbauer experiments of various nuclides. This method is especially suitable for nuclides whose nuclear resonance energy is high. It is originally proposed by Ruby [8] and actually developed by Seto [9]. This method yields the familiar energy spectrum and thus is suitable for the study of materials including two or more compounds containing the nuclide. Moreover, similarly to the NFS method, we are able to use tiny samples and the environmental chambers, owing to the high brilliance of SR. In addition, the requirements on the bunch mode of SR are relaxed for SR-based Mössbauer absorption spectroscopy, compared to the NFS method. One problem is the measuring time; in the first experiment, it took 90 hours to obtain one spectrum [9]. However, this problem was notably alleviated by the development of the new system which enables the detection of internal conversion (IC) electrons [10]. This system is continuing to be improved. In this report, we describe the details of the current measuring system and its properties, and some applications of this method.

2 Experimental

2.1 Experimental system

The schematic drawing of the current measuring system of SR-based Mössbauer absorption spectroscopy is shown in Fig. 1. Any bunch mode of SR except the multi-bunch mode

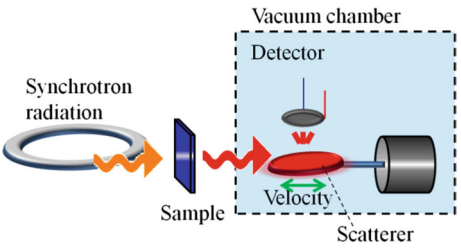

Fig. 1 Schematic drawings of the measurement system of the SR-based Mössbauer absorption spectroscopy. The scatterer and the detector is arranged in the same vacuum chamber to detect the IC electrons

is available in principle because we can take the appropriate time window in those modes, as described later. SR from the undulator is monochromatized appropriately and then it is transmitted through the sample. Here, we can arrange any environmental chamber and/or any X-ray optical techniques, if only SR is transmitted the sample. For example, we can use a high pressure cell or a gas chamber. We can also use thin film samples in combination with the total reflection technique. Downstream of the sample, SR is scattered by an energy standard scatterer, with the energy profile of a simple single-line. Furthermore, its resonance energy is controlled by a conventional velocity transducer. In addition, it is strongly desirable that the recoilless fraction of the scatterer is high. To select a suitable scatterer that satisfies these conditions, it is very useful to consider the chemical species used as γ-ray sources in conventional Mössbauer spectroscopy. Moreover, we can apply other species, whose chemical composition is broken by the α-decay or β-decay of the parent nuclides in conventional RI Mössbauer spectroscopy. The next component to the scatterer is the APD detector just above the scatterer. The nuclear resonant scattering (NRS) from the scatterer is detected by it. The NRS is separated from the enormous prompt electronic scattering by taking an appropriate time window. At the APD, the nuclear resonance γ-rays, the IC electrons, and fluorescent X-rays and Auger electrons after the IC process are detected as the NRS. The detector and the scatterer are arranged in the same vacuum chamber, to detect the electrons. Because the IC coefficients of many Mössbauer nuclides are higher than 1, the detection of electrons results in substantial enhancement of the counting rate of the NRS in SR-based Mössbauer absorption spectroscopy of these nuclides. Moreover, this system has another advantage for the spectroscopy of all Mössbauer nuclides. It is the close distance between the scatterer and the detector, owing to the absence of the X-ray windows. This closeness yields a large solid angle of the detector surface subtended at the scattering point and thus results in efficient detection. In the current system this distance was typically 4 mm. When we assume that the scattering from the scatterer comes from a point and an 8-element APD, where each element has the size of 3 $\times$5 mm ^{2}, is arranged perpendicular to the shortest path of the scattering, the solid angle is 1.8 sr. The actual effect of these two properties is described in Section 3.3. Using this measurement system, the dependence of the intensity of the NRS on the velocity of the scatterer is observed. In fact, when the nuclear resonance energy of the scatterer coincides with the resonance energy of the transmitter, the SR after the transmitter at the energy reduces owing to the nuclear absorption by the transmitter and the NRS from the scatterer also reduces; in contrast, when the nuclear resonance energy of the scatterer does not coincides with the resonance energy of the transmitter, the SR from the transmitter at the resonance energy of the scatterer does not reduces and the NRS from the scatterer also does not reduce. In this way, the energy-domain Mössbauer absorption spectrum is observed.

2.2 Analysis

The statement on the absorption spectrum in the former section is correct only in the simplest case. In the actual case, we should consider the effects of the time window and nuclear resonant forward scattering by the transmitter. In the case of a single component, the actual spectra $I(w_s)$ as a function of the resonance frequency of the scatterer w_s will be of the following form[9, 11–13] :

$$I(w_s) = I_A(w_s) + I_C(w_s) + I_B, \tag{1}$$

$$I_A(w_s) = C_A \int_{\tau_1}^{\tau_2} d\tau \int_0^{z_s} dz \left| \int \frac{dw}{2\pi} \frac{\exp(-iw\tau)}{w - w_s + i/2} E_t(w) E_s(w, w_s, z) \right|^2, \tag{2}$$

$$I_C(w_s) = C_C \int_{\tau_1}^{\tau_2} d\tau \int_0^{z_s} dz \left| \int \frac{dw}{2\pi} \exp(-iw\tau) [E_t(w) E_s(w, w_s, z) - 1] \right|^2, \tag{3}$$

$$E_t(w) = E_{0t} \exp\left(-\frac{\mu_{et} z_t}{2}\right) \exp\left(-i \sum_m \alpha_m \frac{\mu_{nt} z_t}{2[2(w - w_{tm}) + i]}\right), \tag{4}$$

$$E_s(w, w_s, z) = E_{0s} \exp\left(-\frac{\mu_{es} z}{2}\right) \exp\left(-i \frac{\mu_{ns} z_t}{2[2(w - w_s) + i]}\right). \tag{5}$$

Here, I denotes the intensity of the total Mössbauer spectrum, I_A denotes the intensity of the process in which the scattering from the scatter is due to the nuclear resonant scattering, I_C denotes the intensity of the process in which the scattering from the scatter is due to the emission after the photoelectric absorption, and I_B denotes the intensity of the other process independent of w_s, such as the nuclear resonant absorption with recoil at the scatterer. In addition, C_A and C_C are constants; τ_1 and τ_2 are the starting and ending times, respectively, of the time window in units of the lifetime of the nuclear excited state; z_t (z_s) denotes the thickness of the transmitter (scatterer); i denotes the imaginary unit; E_t (E_s) denotes the propagating coherent field amplitudes of the transmitter (scatterer); E_{0t} (E_{0s}) denotes the amplitude of the radiation field at the entrance of the transmitter (scatterer); μ_{et} (μ_{es}) denotes the electronic absorption coefficient of the transmitter (scatterer); μ_{nt} (μ_{ns}) denotes the linear absorption coefficient of radiation by the nuclei at resonance in the transmitter (scatterer); the index m denotes a nuclear transition in the transmitter; α_m and w_{tm} denotes the transition probability ratio and the resonance energy for the mth transition at the transmitter. In the case of multi-components, the sum over components is added in (4). These formulae provide the simple and familiar Lorentzian function in the limit of thin samples, when the term I_C is ignored and the time window is $[0, +\infty]$. When the time window is finite, the spectra are modified. Figure 2 shows an example of the measured spectra with different time windows [13]. As shown in this figure, there are two effects: the narrowing of the energy width and the wavy pattern in the background. The narrowing effect is advantageous to the case where the nuclear hyperfine structure is small and precise analysis is required. In contrast, the wavy pattern of the background is a drawback; it may conceal small components, in its first look. The detailed analysis using the (1) - (5) reveals the small components. In addition, when we observe the spectra obtained at different time windows, the wavy pattern changes, while the energy of the absorption by small components remains unchanged; thus we can see small components experimentally by the comparison of the spectra with different time window. Here, we also note when a spectrum includes only one or two components and their hyperfine structure is simple, the analysis with a Lorentzian function still yields the correct results for the hyperfine parameters. This is the case in Section 3.2.

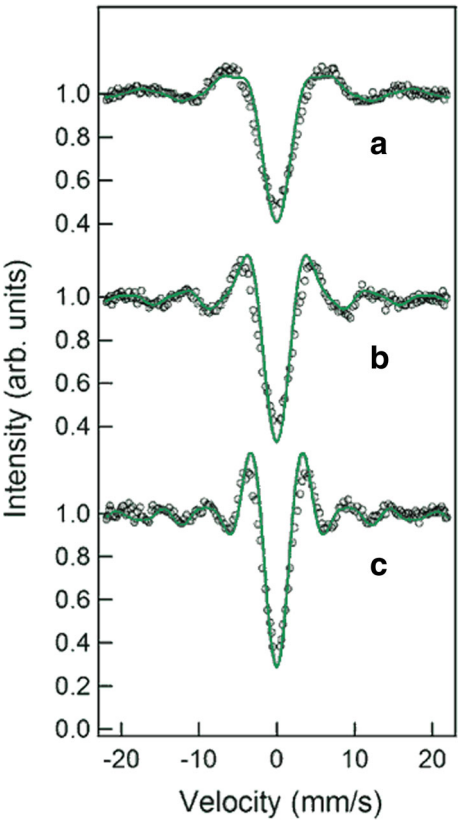

Fig. 2 SR-based Mössbauer spectra of ^{151}Eu in natural EuF_3 used as a transmitter (40 μm thickness) and a scatterer (30 μm thickness) with time windows of (**a**) from 5.7 to17.0 ns, (**b**) from 8.1 to 17.0 ns and (**c**) from 10.5 to 17.0 ns, cited from ref. 13. (Note the half-life of ^{151}Eu 1st state is 9.6 ns.) Lines represent the spectra calculated by (1)-(5)

3 Applications

This system has already been applied to many applications. In fact, SR-based Mössbauer absorption spectroscopy of ^{40}K [14], ^{61}Ni [15], ^{73}Ge [9], ^{119}Sn [16], ^{125}Te [17], ^{127}I, ^{149}Sm, ^{151}Eu [13], ^{174}Yb [10], and ^{189}Os [18] has been performed. Here, some applications are introduced with a focus on the conditions and the results.

3.1 ^{40}K [14]

This system is applied to the study of the magnetism of potassium nano-clusters. Although potassium does not have the d- or f-electrons, the magnetic order induced from potassium was reported in the potassium nano-clusters in the cage of the aluminosilicate porus crystal of zeolite, $(AlSiO_4)_3$, by using several experiments, such as the magnetization measurement, μSR, and ^{27}Al-NMR [19–22]. However, they are indirect methods to confirm the potassium-induced magnetization. To confirm the existence of the potassium induced magnetization, ^{40}K Mössbauer spectroscopy is more powerful method. However, there are no appropriate parent nuclides for the γ-ray source of ^{40}K. Furthermore, the sample amount is limited because of the synthesis method. Therefore, SR-based Mössbauer absorption spectroscopy was performed to validate the magnetism by potassium. The experiments were performed at the BL09XU beamline of SPring-8. The SR was monochromatized to the

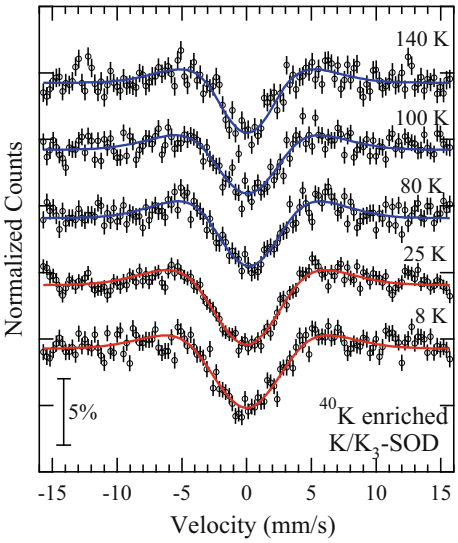

Fig. 3 The ^{40}K SR-based Mössbauer absorption spectrum of potassium nano-clusters at various temperatures, cited from ref. 14. The Néel temperature of this nano-cluster is 72 K. The blue and red lines are the spectra calculated by the (1)-(5)

bandwidth of 200 meV full width at half maximum (FWHM) around the ^{40}K nuclear resonance by using the Si (12 8 4) monochromator. The sample was the potassium nanoclusters in the sodalite cages, where the enrichment of ^{40}K was 4.7 %. The energy standard scatterer was ^{40}KCl at 38K, where the enrichment was 4%. The KCl sample was also used as the energy standard of the ^{40}K Mössbauer spectroscopy using the in-beam method [23]. The results are shown Fig. 3. Careful analysis including the temperature dependence of the recoilless fraction showed the internal magnetic field at ^{40}K. In fact, the hyperfine magnetic field of 9.2 ±3.0 T is observed at 8 K. Because the zeolite cage alone does not show any magnetism, there should be no transferred hyperfine field. This hyperfine magnetic field is so strong that it cannot be the dipole contribution from the magnetic impurity, which was another candidate for the magnetism observed by bulk measurement. Therefore, this signifies the spontaneous polarization of *s*-electron spins in potassium under the anti-ferromagnetic ordering.

3.2 ^{151}Eu [24]

This system was also applied to the study of europium hydride under high hydrogen pressure using a diamond anvil cell (DAC). Thus far, the known europium hydride is EuH_2 with an orthorhombic structure at low hydrogen pressure, less than 6.1 MPa [25]. This structure is irregular in the rare-earth hydride because the structure of the other rare-earth hydrides REH_x (x>2) are hexagonal-closed packed (hcp) or face-centered cubic (fcc) structure. However, a new europium hydride phase was discovered under high hydrogen pressure by X-ray diffractions [24]. The structure above 9.7 GPa hydrogen pressure has the body-centered tetragonal structure, which is similar to the fcc structure. To elucidate the mechanism of the synthesis of this new hydride, SR-based Mössbauer absorption spectroscopy was performed at the BL09XU beamline of SPring-8. The SR was monochromatized to the bandwidth of 2.0 meV FWHM around the ^{151}Eu nuclear resonance by using a Si high resolution monochromator. The sample was natural europium metal at room temperature in the DAC with the hole size of the gasket of approximately 100 μm. The hydrogen fluid was also

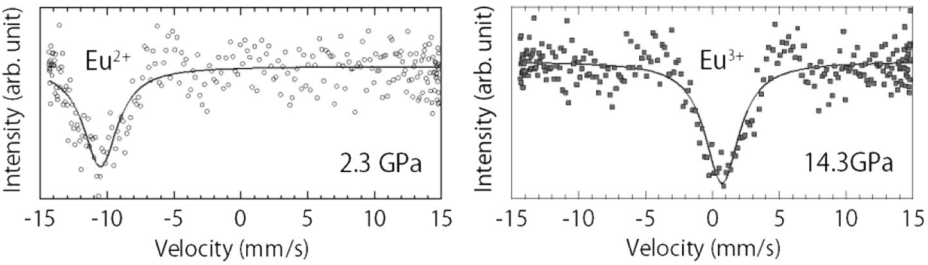

Fig. 4 The ^{151}Eu SR-based Mössbauer absorption spectrum of europium hydride, cited from ref. 20. The left graph is normal europium hydride at 2.3 GPa hydrogen pressure and the right graph is newly discovered hydride at 14.3 GPa hydrogen pressure. The lines are spectra estimated by using a Lorentzian funciton. For these spectra, the Lorentzian fitting is sufficient to see the valence of Eu

packaged in the DAC as both the pressure medium and hydrogen source. The energy standard scatterer was natural EuF_3 at room temperature. The EuF_3 was used as the energy standard in the ^{151}Eu Mössbauer spectroscopy with a γ-ray source and the isomer shift relative to EuF_3 was studied for many Eu compounds [23]. The results are shown in Fig. 4; the right figure shows the spectrum of the Eu hydride at 2.3 GPa hydrogen pressure and the left shows that of the Eu hydride at 14.3 GPa. The nuclear resonance energy clearly changed between the normal and new hydride. In fact, the change was very simple and clear, and the rough analysis with the Lorentzian function instead of the (1)-(5) was sufficient; the isomer shift at 2.3 GPa hydrogen pressure was -10.50 mm/s, while that at 14.3 GPa hydrogen pressure was 0.71 mm/s. This means the hydride at high hydrogen pressure showed a 3+ valence state, while the normal hydride showed a 2+ valence state. This clearly shows that hydrogen penetration induces the valence transition of Eu hydride and implies that the new hydride can be written as EuH_x ($x>2$). When we consider that the other rare-earth elements take the 3+ valence state in their hydride REH_x ($x>2$), the hydrogenation process of Eu is no longer the irregular in the rare-earth element.

3.3 ^{174}Yb [10]

This system was also applied to the ^{174}Yb Mössbauer spectroscopy [10]. Although ^{174}Yb is the most abundant isotope (31.8%), ^{170}Yb (natural abundance of only 3 %) is the most popular nuclides in Yb RI Mössbauer spectroscopy owing to the convenience in the preparation of its γ-ray source [23]. However, the problem of the RI preparation is no concern with SR experiments and thus ^{174}Yb SR-based Mössbauer absorption spectroscopy was performed. The actual experiments were performed at the BL09XU and BL11XU beamlines of SPring-8. Appropriately monochromatized SR was transmitted through the natural YbB_{12} sample and then was scattered by the natural YbB_{12} scatterer. YbB_{12} was used here because $^{170}TmB_{12}$ was a single-line γ-ray source species in RI ^{170}Yb Mössbauer spectroscopy. Here, two experiments were performed to compare the effect of electron detection; the first experiment was performed by the system similar to that in the first experiments in Ref. [9], that is, without electron detection, and the second was by the system with electron detection, as described in Section 2. The temperatures of the sample and scatterer were 13.5 K and 20 K in the first experiment, respectively, and 20 K and 26 K in the second experiment respectively. The obtained spectra are shown in Fig. 5; Fig. 5a is the spectrum measured in 11 hours by the system without electron detection and Fig. 5b is the spectrum measured in 10 hours by the system with electron detection. Although the measuring time is less and the

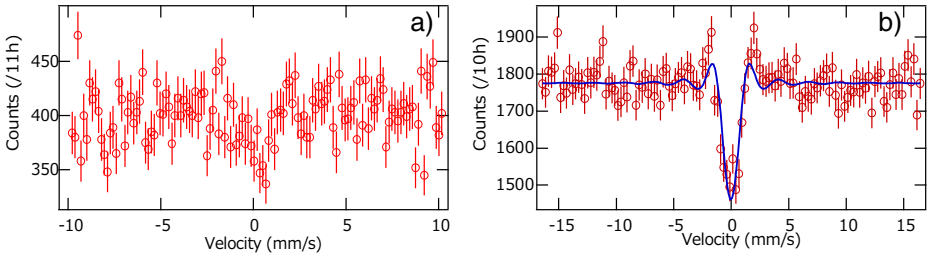

Fig. 5 The ^{174}Yb SR-based Mössbauer absorption spectra of YbB_{12}. The right graph 5b is cited from ref. 10. The left graph 5a is the spectrum by the system without electron detection and the 5a is the spectrum by the system with electron detection. The blue line is the spectrum calculated by the (1)-(5). In Fig. 5a, the absorption should be seen around the velocity zero, although a large statistical error is included

recoilless fraction should be slightly lower due to the slightly high temperature, the spectrum by the system with electron detection is by far clearer. Owing to the insufficient counts, the statistical error in Fig. 5a is so large that the evaluation by (1)-(5) is unstable. In contrast, we can clearly evaluate Fig 5b. In fact, the counting rate of the detector was 6 counts per second (cps) in the current system, while that had been 1.2 cps in the system without electron detection. This clearly shows the effectiveness of the current system with electron detection. Here, we note that the enhancement is due to both the electron detection and the closeness of the distance between the detector and the scatterer. The distances were 5 mm and 7 mm in the system with and without electron detection, respectively. This difference corresponds to the 1.3 times contribution to the enhancement. However, the counting rate with electron detection was 5 times as high as the rate without electron detection. Thus, the contribution of the electron detection was roughly 4 times enhancement and the electron detection is the major component in this enhancement. We also note that the spectrum in Fig. 5b shows the width-narrowing effect arising from the time window. In fact, when the FWHM of Fig. 5b is estimated by the Lorentzian function, it is 1.3 mm/s, while the FWHM of the spectrum in the usual RI Mössbauer spectroscopy is not less than 2.0 mm/s, which is the twice of the natural line width of ^{174}Yb. This width narrowing effect is advantageous for the evaluation of the ^{174}Yb isomer shift, because the difference between the isomer shift of Yb^{2+} ($YbSO_4$) and that of Yb^{3+} ($Yb_2(SO_4)_3 \bullet 8H_2O$) was 0.43 ±0.14 mm/s [26] and the valence of the Yb element directly concerns the property of Yb compounds, like the Kondo effect and the RKKY interaction.

4 Discussion

As shown above, many nuclides are now available for this method. Moreover, there are many potentially available nuclides. In fact, this method is relatively advantageous for the nuclides with high IC coefficient and high resonance energy, such as ^{155}Gd and ^{166}Er. We are now planning to accomplish SR-based Mössbauer spectroscopy with these potentially available nuclides.

Moreover, this system also continues to be developed for the convenience of the actual experiment. To save the expensive liquid helium coolant, a He-gas exchange refrigerator is now combined with this system for the cooling of the energy standard scatterer. Moreover, a new scintillation detector for high energy X-rays is tried in the SR-based Mössbauer absorption spectroscopy of ^{61}Ni, the IC coefficient of which is only 0.139 [15].

We also note this arrangement is effective for the nuclear resonant inelastic scattering (NIS) experiments. The arrangement of the scatterer and the detector in this system is the same as the arrangement of the sample and the detector in NIS experiments. Both the detection of electrons and the large solid angle will improve the measuring time of the NIS spectrum.

Now we note that the time domain method of SR, like NFS, and the energy domain method of SR, like the SR-based Mössbauer absorption spectroscopy and synchrotron Mössbauer source (SMS) [27–29] are in complementary relation. The optimal method depends on the sample and objective under study. When we study the fundamental physics or require a precise evaluation, NFS is usually favorable, because the time spectrum is sensitive to the phase of the coherent scattering and we can evaluate the precise hyperfine structure. In contrast, when we study complex materials including many components, the energy spectrum method is often preferred because we can intuitively select the analyzing model. Especially, we need not arrange the time window in SMS and need not consider the resultant effect, although the SMS can be used only for ^{57}Fe. However, this is only the general trend. In fact, we can obtain the exact hyperfine parameters by all these methods, in principle. Even the isomer shift can be obtained in NFS by using a reference sample [30]. The combination of the time-domain method and the energy-domain method will further extend the applicability of the Mössbauer effect.

5 Summary

The details of the arrangement of the current SR-based Mössbauer absorption spectroscopy system are described. The properties of the current system for electron detection are the following two: the detection of IC electron as well as the X-rays, and the efficient detection owing to the close distance between the scatterer and the detector. The observed spectra can be analyzed by the (1)-(5). The time window affects the following two properties of the spectra: the width narrowing and the wavy pattern in the background. Now the SR-based Mössbauer spectroscopy of ^{40}K, ^{61}Ni, ^{73}Ge, ^{119}Sn, ^{125}Te, ^{127}I, ^{149}Sm, ^{151}Eu, ^{174}Yb, and ^{189}Os has been already performed. In the case of ^{40}K, although the sample was nanoclusters and its amount was limited, the spectra were successfully obtained and they showed the spontaneous polarization of s-electron spins of potassium under the anti-ferromagnetic order. In the case of ^{151}Eu, although the sample was Eu hydrides in the DAC and its sample size was small, the spectrum was successfully obtained and showed the valence transition due to the hydrogen penetration. In the case of ^{174}Yb, the increase of the counting rate by the system with electron detection is shown and the importance of the width-narrowing effect is discussed. The continued development of this system is also described, including the combination of the refrigerator and/or the new detector for high energy X-rays. In addition, the applicability of the arrangement of this system to NIS experiments is discussed. The complementary relation of the time domain method and energy domain method is also noted. The optimal method depends strongly on the sample and the objective of study.

Acknowledgments The authors would like to thank Professor S. Kishimoto of High Energy Accelerator Research Organization for all his valuable advice during the development of the electron detection system. We would also like to thank the Accelerator Group of SPring-8 for their support, especially with the top-up injection operation. These experiments and developments were performed at the BL09XU and BL11XU beamlines of SPring-8 with the approval of the Japan Synchrotron Radiation Research Institute (JASRI) (Power User Priority Program Nos. 2012A0086 and 2013A0086 and Proposal Nos. 2010B1244 and 2011B1054 and No.2012B1238 for BL09XU, and Proposal Nos. 2011B3501, 2012A3501 for BL11XU).

This work has been supported by JSPS KAKENHI Grant-in-Aid for Scientific Research (S) of Grant No. 24221005.

References

1. Gütlich, P., Bill, E., Trautwein, A.X.: Mössbauer spectroscopy and transition metal chemistry. Springer, Berlin (2011)
2. Website of the Mössbauer Effect Data Center: http://www.medc.dicp.ac.cn/Resources.php. Accessed 29 September 2015 (2015)
3. Hastings, J.B., Siddons, D.P., van Bürck, U., Hollatz, R., Bergmann, U.: Mössbauer spectroscopy using synchrotron radiation. Phys. Rev. Lett. **66**, 770–773 (1991)
4. Seto, M., Kitao, S., Kobayashi, Y., Haruki, R., Mitsui, T., Yoda, Y., Zhang, X.W., Kishimoto, S., Maeda, Y.: Nuclear resonant inelastic and forward scattering of synchrotron radiation by ^{40}K. Hyperfine Interact **141/142**, 99–108 (2002)
5. Bessas, D., Sergueev, I., Merkel, D.G., Chumakov, A.I., Rüffer, R., Jafari, A., Kishimoto, S., Wolny, J.A., Schünemann, V., Needham, R.J., Sadler, P.J., Herman, R.P.: Nuclear resonant scattering of synchrotron radiation by ^{187}Os. Phys. Rev. B **91**, 224102 (2015)
6. Sergeev, I., Chumakov, A.I., Deschaux Beaume-Dang, T.H., Rüffer, R., Strohm, C., van Bürck, U.: Nuclear forward scattering for high energy Mössbauer transitions. Phys. Rev. Lett. **99**, 097601 (2007)
7. Bessas, D., Merkel, D.G., Chumakov, A.I., Rüffer, R., Hermann, R.P., Sergueev, I., Mahmoud, A., Klobes, B., McGuire, M.A., Sougrati, M.T., Stievano, L.: Nuclear forward scattering of synchrotron radiation by ^{99}Ru. Phys. Rev. Lett. **113**, 147–601 (2014)
8. Ruby, S.L.: Mössbauer experiments without conventional sources. J. Phys. (Paris), Colloq **35**, C6–209 (1974)
9. Seto, M., Masuda, R., Higashitaniguchi, S., Kitao, S., Kobayashi, Y., Inaba, C., Mitsui, T., Yoda, Y.: Synchrotron-radiation-based Mössbauer spectroscopy. Phys. Rev. Lett. **102**, 217–602 (2009)
10. Masuda, R., Kobayashi, Y., Kitao, S., Kurokuzu, M., Saito, M., Yoda, Y., Mitsui, T., Iga, F., Seto, M.: Synchrotron radiation-based Mössbauer spectra of ^{174}Yb measured with internal conversion electrons. Appl. Phys. Lett. **104**, 082–411 (2014)
11. Smirnov, G.V., Kohn, V.G.: Theory of nuclear resonant scattering of synchrotron radiation in the presence of diffusive motion of nuclei. Phys. Rev. B **52**, 3356–3365 (1995)
12. Smirnov, G.V., van Bürck, U., Arthur, J., Brown, G.S., Chumakov, A.I., Baron, A.Q.R., Petry, W., Ruby, S.L.: Currents and fields reveal the propagation of nuclear polaritons through a resonant target. Phys. Rev. A **76**, 043–811 (2007)
13. Seto, M., Masuda, R., Higashitaniguchi, S., Kitao, S., Kobayashi, Y., Inaba, C., Mitsui, T., Yoda, Y.: Mössbauer spectroscopy in the energy domain using synchrotron radiation. J. Phys. Conf. Ser. **217**, 012–002 (2010)
14. Nakano, T., Fukuda, N., Seto, M., Kobayashi, Y., Masuda, R., Yoda, Y., Mihara, M., Nozoe, Y.: Synchrotron-radiation-based Mössbauer spectroscopy of ^{40}K in antiferromagnetic potassium nanoclusters in sodalite. Phys. Rev. B **91**, 140101R (2015)
15. Kishimoto, S., Nishikido, F., Haruki, R., Shibuya, K., Koshimizu, M.: Fast scintillation detectors for high-energy X-ray region. Hyperfine Interact **204**, 101–110 (2012)
16. Mibu, K., Seto, M., Mitsui, T., Yoda, Y., Masuda, R., Kitao, S., Kobayashi, Y., Suharyadi, E., Tanaka, M., Tsunoda, M., Yanagihara, H., Kita, E.: Studies on spintronics-related thin films using synchrotron-radiation-based Mössbauer spectroscopy. Hyperfine Interact **217**, 127–135 (2013)
17. Kurokuzu, M., Kitao, S., Kobayashi, Y., Saito, M., Masuda, R., Mitsui, T., Yoda, Y., Seto, M.: Development of ^{125}Te synchrotron-radiation-based Mössbauer spectroscopy. Hyperfine Interact **226**, 687–691 (2014)
18. Yamaura, J., Ohsumi, H., Sugimoto, K., Tsutsui, S., Yoda, Y., Takeshita, S., Tokuda, A., Kitao, S., Kurokuzu, M., Seto, M., Yamauchi, I., Ohgushi, K., Takigawa, M., Arima, T., Hiroi, Z.: Phase transition magnetic structure of pyrochlore oxide $Cd_2Os_2O_7$. J. Phys. Conf. Ser. **391**, 012–112 (2012)
19. Damjanović, L., Stucky, G.D., Srdanov, V.I.: Magnetism of F centers; indication of an antiferromagnetic phase transition in potassium-electro-sodalite. J. Serb. Chem. Soc. **65**, 311–314 (2000)
20. Tou, H., Maniwa, Y., Mizoguchi, K., Damjanović, L., Srdanov, V.I.: NMR studies on antiferromagnetism in alkali-electro-sodalite. J. Magn. Magn. Mater. **226-230**, 1098–1100 (2001)
21. Nakano, T., Suehiro, R., Hanazawa, A., Watanabe, K., Watanabe, I., Amato, A., Pratt, F.L., Nozoe, Y.: μSR study on antiferromagnetism of alkali-metal clusters incorporated in zeolite sodalite. J. Phys. Soc. Jpn. **79**, 073–707 (2010)

22. Nakano, T., Tsugeno, H., Hanazawa, A., Kashiwagi, T., Nozoe, Y., Hagiwara, M.: Antiferromagnetic resonance in alkali-metal clusters in sodalite. Phys. Rev. B **88**, 174–401 (2013)
23. Shenoy, G.K., Wagner, F.E.: Mössbauer isomer shifts. North-Holland, Amsterdam (1978)
24. Matsuoka, T., Fujihisa, H., Hirao, N., Ohishi, Y., Mitsui, T., Masuda, R., Seto, M., Yoda, Y., Shimizu, K., Machida, A., Aoki, K.: Structural and valence changes of europium hydride induced by application of high-pressure H_2. Phys. Rev. Lett. **107**, 025–501 (2011)
25. Hardcastle, K.I., Warf, J.C.: Rare earth-hydrogen system III. High pressure Investigations. Inorg. Chem. **5**, 1728–1735 (1966)
26. Henning, W., Bähre, G., Kienle, P.: Isomer shift and quadrupole splitting of the 2^+-rotational state in ^{174}Yb. Z. Phys. **241**, 138–149 (1971)
27. Gerdau, E., Rüffer, R., Winker, H., Tolksdorf, W., Klages, C.P., Hannon, J.P.: Nuclear bragg diffraction of synchrotron radiation in yttrium iron garnet. Phys. Rev. Lett. **54**, 835–838 (1985)
28. Chumakov, A.I., Zelepukhin, M.V., Smirnov, G.V., van Bürck, U., Rüffer, R., Hollatz, R., Rüter, H.D., Gerdau, E.: Time spectra of a nearly-single-line pure nuclear reflection excited by synchrotron radiation. Phys. Rev. B **41**, 9545–9547 (1990)
29. Sminov, G.V., van Bürck, U., Chumakov, A.I., Baron, A.Q.R., Rüffer, R.: Synchrotron Mössbauer source. Phys. Rev. B. **55**, 5811–5815 (1997)
30. Leupold, O., Rupprecht, K., Wortmann, G.: Electronic and magnetic transitions in europium compounds studied by nuclear forward scattering of synchrotron radiation. Structural Chem **14**, 97–107 (2003)